

Branching ratio measurements of the predissociation of 12C16O by timeslice velocity-map ion imaging in the energy region from 108000 to 110500 cm-1

Hong Gao, Yu Song, Lei Yang, Xiaoyu Shi, Qing-Zhu Yin et al.

Citation: J. Chem. Phys. 137, 034305 (2012); doi: 10.1063/1.4734018

View online: http://dx.doi.org/10.1063/1.4734018

View Table of Contents: http://jcp.aip.org/resource/1/JCPSA6/v137/i3

Published by the American Institute of Physics.

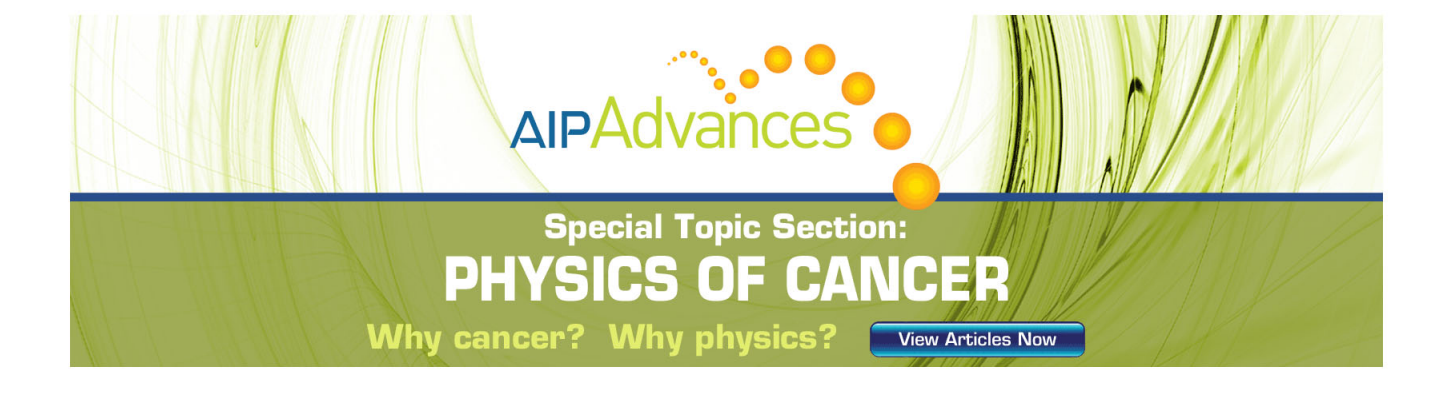
Additional information on J. Chem. Phys.

Journal Homepage: http://jcp.aip.org/

Journal Information: http://jcp.aip.org/about/about_the_journal Top downloads: http://jcp.aip.org/features/most_downloaded

Information for Authors: http://jcp.aip.org/authors

ADVERTISEMENT



Branching ratio measurements of the predissociation of ¹²C¹⁶O by time-slice velocity-map ion imaging in the energy region from 108 000 to 110 500 cm⁻¹

Hong Gao,¹ Yu Song,¹ Lei Yang,¹ Xiaoyu Shi,¹ Qing-Zhu Yin,² C. Y. Ng,^{1,a)} and William M. Jackson^{1,a)}

(Received 1 May 2012; accepted 21 June 2012; published online 17 July 2012)

Direct branching ratio measurements of the three lowest dissociation channels of $^{12}C^{16}O$ that produce $C(^3P) + O(^3P)$, $C(^1D) + O(^3P)$, and $C(^3P) + O(^1D)$ are reported in the vacuum ultraviolet region from $108\,000~cm^{-1}$ (92.59 nm) to $110\,500~cm^{-1}$ (90.50 nm) using the time-slice velocity-map ion imaging and nonlinear resonant four-wave mixing techniques. Rotationally, resolved carbon ion yield spectra for both $^1\Sigma^+$ and $^1\Pi$ bands of CO in this region have been obtained. Our measurements using this technique show that the branching ratio in this energy region, especially the relative percentages of the two spin-forbidden channels, is strongly dependent on the particular electronic and vibrational energy levels of CO that are excited. © 2012 American Institute of Physics. [http://dx.doi.org/10.1063/1.4734018]

I. INTRODUCTION

Carbon monoxide is the second most abundant known molecule after H₂ in the interstellar medium.^{1,2} Because of its chemical stability and many readily detectable physical properties, CO has served as one of the most important tracermolecules in astronomy and astrophysics.3-5 To chemists and physicists, CO and its isoelectronic molecule N₂ are important because they supply benchmark information about the photodissociation dynamics of small molecules. A comparison between the two isoelectronic molecules N2 and CO made by Huber⁶ pointed out that the interactions between different electronic states of CO, especially the Π - Π type, are still largely unknown compared with N2 because the absence of g/u symmetry adds a great deal of complexity. A more recent comparison between these two diatomic molecules, which focuses on their potential energy surfaces (PES) and predissociation mechanisms was reported by Lefebvre-Brion and Lewis.⁷ They pointed out again that more experimental and theoretical efforts are needed for CO. Recent experimental and theoretical works are only beginning to shed light on the predissociation mechanisms and the PES of CO in the vicinity of 100 000 cm⁻¹.

Wolk and Rich⁸ identified the $D'^1\Sigma^+$ state that leads to $C(^3P) + O(^3P)$ at infinity. Its adiabatic potential curve was calculated by Cooper and Kirby⁹ and more recently by Vazquez *et al.*¹⁰ The $D'^1\Sigma^+$ state plays an important role in the predissociation mechanism of CO through homogeneous $^1\Sigma^+$ or heterogeneous $^1\Sigma^-1\Pi$ interactions with the optically excited Rydberg states of CO.^{11–18} The Rydberg-valence interaction between the $B^1\Sigma^+$ and $D'^1\Sigma^+$ states was modeled

to explain the predissociation of the $B^1\Sigma^+$ state. ^{19–22} The next valence $^1\Sigma^+$ state, which is the $C'^1\Sigma^+$ state and correlates to the $C(^1D) + O(^1D)$ limit was also predicted theoretically ⁹ and then observed by Huber and co-workers. ¹⁸

Although there have been many theoretical and experimental studies of the importance of predissociation from the $^{1}\Sigma^{+}$ valence states, the corresponding understanding of predissociation mechanisms through singlet or triplet states with Π symmetry are still unknown. Some of the low-lying Rydberg states with Π symmetry, which adiabatically transfer to other valence type states at large nuclear distance have been calculated by Cooper and Kirby. 9,23,24 They have not yet been identified in any experiments, although many of the experimental measurements 11,12,14–18,25 implied the existence of repulsive valence states with ${}^{1}\Pi$ or ${}^{3}\Pi$ symmetry. This was based upon the observation that the predissociation of many Rydberg states with Π symmetry do not show any J dependence. 11,25 An even stronger evidence for repulsive valence states with Π symmetry is that the f parity levels show evidence for global predissociation. 11,16 These observations cannot be explained by the heterogeneous interaction with the $D^{\prime 1}\Sigma^{+}$ state, so there must be a homogeneous interaction with the ${}^{1}\Pi$ - ${}^{1}\Pi$ or ${}^{1}\Pi$ - ${}^{3}\Pi$ type. The first valence type ${}^{3}\Pi$ state designated as $k^3\Pi$ was identified by Baker et al., ²⁶ where the $k^3\Pi$ state was employed to explain the accidental predissociation in their REMPI spectrum of the $E^1\Pi$ state. The $k^3\Pi$ state was then reanalyzed and the vibrational levels were reassigned by Berden et al.²⁷ The $k^3\Pi$ state, which predissociates by an unidentified repulsive ${}^{3}\Pi$ states, is found to be responsible for accidental predissociation of many CO states in the energy region below 100 000 cm⁻¹. Baker and co-workers studied the interactions between the $k^3\Pi$ state and $E^1\Pi$, E^2 E^3 and $c^3\Pi$ (Ref. 29) states. Ubachs and co-workers performed detailed investigations on the predissociation mechanism of the $E^1\Pi$ state, 30,31 and its interaction with the $k^3\Pi$ state is

¹Department of Chemistry, University of California Davis, Davis, California 95616, USA

²Department of Geology, University of California Davis, Davis, California 95616, USA

a) Authors to whom correspondence should be addressed. Electronic mail: cyng@chem.ucdavis.edu and wmjackson@ucdavis.edu.

Hill et al.³² reported preliminary calculations for the potential curves for the ${}^{3}\Pi$ states going to the dissociation limit of $C(^{1}D) + O(^{3}P)$. The first direct observation of the predissociation of CO into the triplet channel $C(^{1}D) + O(^{3}P)$ was reported by Okazaki et al.33 by observing the photofragment spectra detecting both C(³P and ¹D) and O(³P) atom fragments. Later the predissociation of CO into the triplet channel $C(^{1}D) + O(^{3}P)$ through a two photon excitation of a $^{3}\Pi$ Rydberg state of CO was reported by Bakker and Parker³⁴ by using the combination of a tunable ArF excimer laser and velocity-map ion imaging setup. The kinetic energy release and the angular distribution of the photofragment for the channel $C(^{1}D) + O(^{3}P)$ were obtained. A predissociation mechanism involving repulsive ${}^{3}\Pi$ states was proposed. A more detailed study by Okazaki et al. 16 showed that the two channels $C(^3P) + O(^3P)$ and $C(^1D) + O(^3P)$ are competitive with comparable rates. Useful information about the branching ratio between the two channels was obtained by comparing the three $C(^{3}P)$, $C(^{1}D)$, and $O(^{3}P)$ ion yield spectra to the simulated absorption spectra. However, they could not distinguish directly the $C(^{3}P) + O(^{3}P)$ channel from the $C(^{3}P)$ $+ O(^{1}D)$ channel since they did not observe $O(^{1}D)$. This product has never been experimentally observed and the branching ratios for the three lowest dissociation channels are still unknown.

We recently reported on a preliminary study of the direct vacuum ultraviolet (VUV) photodissociation of CO to determine the branching ratio for spin allowed and forbidden channels.³⁵ These branching ratios are important for both astronomers and chemists. The ratio between O(³P) and O(¹D) is important in understanding how the CO predissociation products are distributed and locked up in the molecular clouds and the proto-solar nebula, which will be the focus of a separate article.³⁶ To chemists, knowing the relative percentage into the two triplet dissociation channels will help us understand the details of intersystem crossing (spin-orbit coupling) and the Rydberg-valence interactions in light molecules, where high quality theoretical calculations are possible. The experimental results should also be very helpful in identifying the unknown repulsive singlet and triplet Π states that are responsible for the final spin allowed and forbidden products. Finally, all theoretical calculations or simulations of the predissociation rates of CO based on the results from the line-width or the pump-probe decay time measurements have to take into account the contributions of the two triplet channels to the total predissociation rates because these measurements cannot distinguish among the three atomic channels. The methods that have previously been applied to study the photodissociation of CO_2 , 37 N_2 , 38 and NO (Ref. 39) are used in the present paper to study the predissociation of CO in the energy region from $108\,000~\text{cm}^{-1}$ (92.59 nm) to $110\,500~\text{cm}^{-1}$ (90.50 nm).

II. EXPERIMENT

A detailed description of the VUV source photodissociation time-slice velocity-map ion imaging apparatus has been previously provided^{40,41} and will only be briefly summarized here. A pulsed molecular beam of pure CO is produced by supersonic expansion through an Evan-Lavie pulsed valve (EL-5-2004) with a nozzle diameter of 0.2 mm operating at 50 psi and 30 Hz. Two conical skimmers collimate the pulse beam prior to its entrance into the photodissociation/photoionization (PD/PI) region to intersect the VUV beam in a perpendicular direction. The distance between the nozzle and the interaction region is \sim 15 cm. The nascent photofragments and the parent molecules are photoionized by the same VUV laser in the PD/PI region. They are all extracted and focused by the velocity-map ion optics onto a 7.5 cm diameter micro-channel plate (MCP) detector. The electrons from this MCP detector are accelerated to a phosphor screen where the image is recorded with a CCD camera. The electron signal is also coupled out of the MCP and monitored with a digital oscilloscope. The molecular beam will fly along the axis of a 72 cm field-free TOF mass spectrometer before striking a MCP detector. Any metastable neutral atoms or molecules formed in the interaction region by the laser beams takes $\sim 500 \,\mu s$ before they arrive at MCP detector, well after the arrival of all of the ions formed in the PD/PI region.

The tunable VUV laser radiation generation system has also been described. 42 Three VUV beam sources, i.e., $2\omega_1+\omega_2$, $2\omega_1-\omega_2$, and $3\omega_1$ are generated when the ω_1 and ω_2 beams are focused into the T-shaped chamber that is 27.3 cm away from the PD/PI region. Here, the nonlinear gas Kr is introduced into the T-shaped chamber through a general valve operating at 30 Hz. There is no separation lens between the T-shaped chamber and the PD/PI region so all the VUV, UV, and visible laser beams will enter this region through a Teflon aperture with a diameter of 2 mm that is ~8 cm from the center of the interaction region. The VUV laser source is parallel to the plane of the MCP detector. When collecting the carbon ion yield spectrum, the visible laser (ω_2) is scanned from 609 nm to 720 nm with a step size of 0.01 nm and the UV laser (ω_1) is fixed at 212.556 nm. The signal from the MCP detector goes to the input of a Stanford Research Systems (SRS) Boxcar data acquisition system that is gated so that only C⁺ ions are recorded. In the time-slice velocitymap ion-imaging mode, the sum-frequency VUV is fixed to one of the rovibronic states of CO then a high voltage pulse with a width of 40 ns is applied to the front MCP when the

carbon ions arrive. The image from the CCD camera is collected using a computer-based program DaVis7 supplied by LaVision. In this experiment, the CO molecule first absorbs a sum-frequency VUV photon $(2\omega_1+\omega_2)$ and is excited to one of the rovibronic states that undergo predissociation to produce carbon atoms in the ³P and ¹D states. A second VUV photon from the same source ionizes the carbon atoms in the ³P and ¹D states because in this region the energies of the photons that are being used are above the ionization potentials of both of the states of the C atom.

III. EXPERIMENTAL RESULTS

The total kinetic energy release (TKER) spectra are obtained from the time-slice velocity-map ion images and the kinetic energies of each of them are used to identify the three possible dissociation channels, i.e., $C(^3P) + O(^3P)$, $C(^1D) + O(^3P)$, and $C(^3P) + O(^1D)$. Once each of the peaks has been assigned to a particular dissociation channel, the areas under the peaks of the TKER spectra are used to obtain the branching ratios. The $C(^3P) + O(^1D)$ and $C(^3P) + O(^3P)$ channels share the same nascent $C(^3P)$ product, thus the areas of the peaks in the TKER spectra are a direct measure of their relative percentages. For the $C(^1D) + O(^3P)$ channel, the photoionization cross section for the $C(^1D)$ will be different than it is for the $C(^3P)$ so the branching ratio for this channel has to be corrected for the ratio of the photoionization cross sections.

The VUV photons that ionize these carbon atoms are the resonant sum-frequency VUV photons $(2\omega_1+\omega_2)$, rather than the tripling $(3\omega_1)$ photons because the former is more intense. This is confirmed by determining the change in the intensity of the H₂O photoionization peak in the TOF spectrum, with and without the presence of the visible laser, ω_2 . The photoionization cross sections of H₂O at these two frequencies are nearly the same⁴³ and when the visible laser is blocked the peak corresponding to H₂O disappears. This proves that the $2\omega_1+\omega_2$ VUV laser source is much greater than the $3\omega_1$ laser source. In Secs. III A and III B, results for the branching ratio determinations for $^1\Sigma^+$ and $^1\Pi$ bands in the region from $108\,000~{\rm cm}^{-1}$ (92.59 nm) to $110\,500~{\rm cm}^{-1}$ (90.50 nm) are described.

We have found that, for some of the observed bands in this energy region, the assignments from the previous published journal articles are different from the assignments made by Michael Casey in his Ph.D. dissertation in 1979.44 Here in this paper, we will accept the assignments from the published journal articles except where specified and we will put the assignments made by Michael Casey in square brackets where they are different. The photofragment excitation spectra of the C⁺ fragment produced from the predissociation of CO in the energy region from $108\,000 \text{ cm}^{-1}$ (92.59 nm) to $110\,500 \text{ cm}^{-1}$ (90.50 nm) are shown in Figs. 1-4. In these spectra, we observed six ${}^{1}\Sigma^{+}$ bands and six ${}^{1}\Pi$ bands. All of the bands have been identified except for two of the ${}^{1}\Pi$ bands. The results obtained for four of these bands, namely, the $(4s\sigma)^1 \Sigma^+ (v' = 4) [(B^2 \Sigma^+) 3s\sigma, v' = 0]$ and $(4p\sigma)^1 \Sigma^+ (v' + 1) \Sigma^+ ($ = 3) bands and the W(3s σ)¹ Π^+ (v' = 3) and ¹ Π^+ (v' = 2)

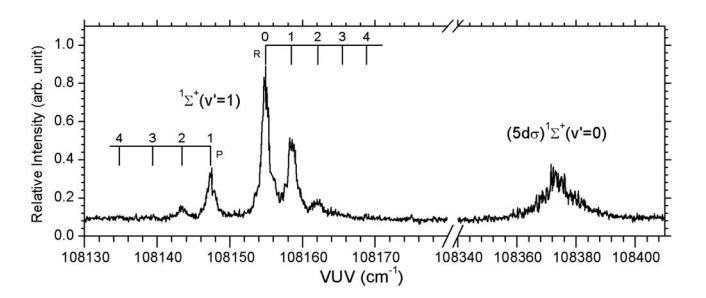


FIG. 1. The C⁺ photofragment spectrum produced from the predissociation of CO following the absorption of a single sum-frequency VUV photon for the bands $^{1}\Sigma^{+}(v'=1)$ [$(4d\sigma)^{1}\Sigma^{+}(v'=1)$] (left) and $(5d\sigma)^{1}\Sigma^{+}(v'=0)$ (right) from 108 130 cm⁻¹ to 108 410 cm⁻¹. The drop line assignments were calculated according to the rotational constants in Ref. 3. The relative intensity of the spectrum is not normalized according to the VUV intensity.

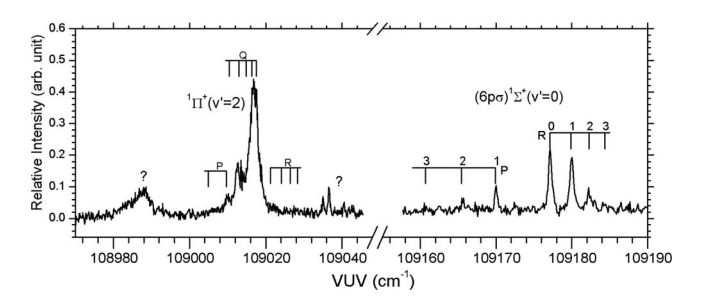


FIG. 2. The C⁺ photofragment spectrum produced from the predissociation of CO following the absorption of a single sum-frequency VUV photon for the bands $^1\Pi(v'=2)$ [(A $^2\Pi)3s\sigma$, v'=4] (left) and (6p\sigma) $^1\Sigma^+(v'=0)$ (right) from 108 970 cm $^{-1}$ to 109 190 cm $^{-1}$. The drop line assignments for $^1\Pi(v'=2)$ [(A $^2\Pi)3s\sigma$, v'=4] (left) were calculated according to the rotational constants in Ref. 3 and the drop line assignments for (6p\sigma)^1\Sigma^+(v'=0) (right) are from Ref. 13. The two reproducible structures labeled by question marks are not yet identified. The relative intensity of the spectrum is not normalized according to the VUV intensity.

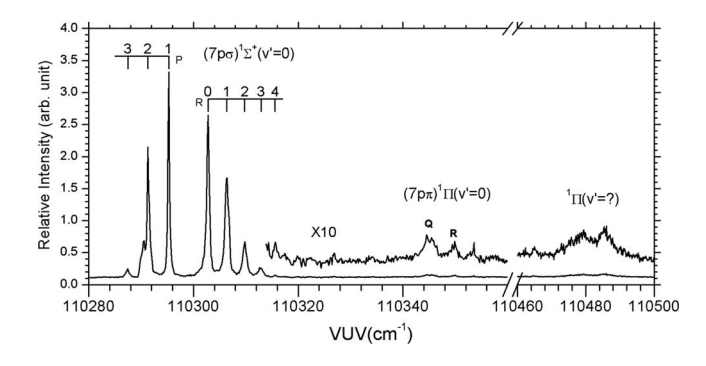


FIG. 3. The C⁺ photofragment spectrum produced from the predissociation of CO following the absorption of a single sum-frequency VUV photon for the bands $(7p\sigma)^1\Sigma^+(v'=0)$ (left), $(7p\pi)^1\Pi(v'=0)$ (middle) and ${}^1\Pi(v'=?)$ (right) from $110\,280\,\mathrm{cm}^{-1}$ to $110\,500\,\mathrm{cm}^{-1}$. The drop lines show the assignments for the band $(7p\sigma)^1\Sigma^+(v'=0)$ (left). The spectrum above $110\,312\,\mathrm{cm}^{-1}$ was amplified by a factor of 10 to show in the figure. The relative intensity of the spectrum is not normalized according to the VUV intensity.

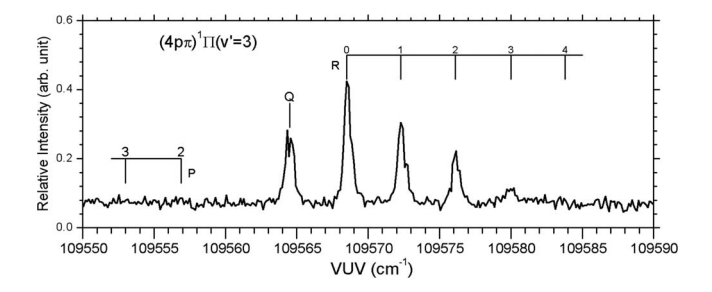


FIG. 4. The C⁺ photofragment spectrum produced from the predissociation of CO following the absorption of a single sum-frequency VUV photon for the band $(4p\pi)^1\Pi(v'=3)[(A^2\Pi)3p\sigma v'=0]$ from $109\,550~{\rm cm}^{-1}$ to $109\,590~{\rm cm}^{-1}$. The drop line assignments were obtained from Ref. 13. The relative intensity of the spectrum is not normalized according to the VUV intensity.

 $[(A^2\Pi)3s\sigma, v'=4]$ bands, have already been reported in a recent communication.³⁵

A. $^{1}\Sigma^{+}$ bands

The C⁺ photofragment excitation spectrum in the region between 108 130 and 108 410 is shown in Fig. 1. The first band at 108 150 cm⁻¹ was observed in the absorption spectrum by Letzelter *et al.*⁴⁵ and labeled as 11 in Table I of Ref. 45 as a $^{1}\Sigma^{+}$. It was assigned as $(4d\sigma)^{1}\Sigma^{+}$ (v'=1) by Casey.⁴⁴ Its band origin and rotational constants were reported by Eidelsberg and Rostas.³ Our assignments of the rotational levels shown by drop lines in Fig. 1 were calculated using the rotational constants in Ref. 3. From the spectrum, we can see that the rotational lines are obviously broadened due to the predissociation process. This is consistent with an excited state life time of the order of 10^{-11} s reported by Eidelsberg and Rostas.³

The second ${}^{1}\Sigma^{+}$ band is $(5d\sigma){}^{1}\Sigma^{+}(v'=0)$ and was reported as a diffuse band without any resolved rotational structure by both Eidelsberg and Rostas³ with a life time of the order of 10^{-12} s and by Okazaki et al. ¹⁶ in their C(³P) ion yield spectrum. We also see this diffuse band in our C⁺ photofragment spectrum at $108\,374.0\,\mathrm{cm}^{-1}$ in Fig. 1, but the full-width at half-maximum of this band corresponds to a predissociation lifetime of 4×10^{-13} s. This is a factor of 2.5 faster than the previously reported value and it is too fast for us to observe any rotational structure in the C⁺ photofragment spectrum. According to the Table I in Ref. 5, the next two ${}^{1}\Sigma^{+}$ are $I'(5s\sigma)^1\Sigma^+(v'=1)$ and $(6s\sigma)^1\Sigma^+(v'=0)$ which should be at 108 679.0 cm⁻¹ and 108 789.1 cm⁻¹, respectively. We did not see these two bands in our C⁺ photofragment spectrum probably because the sum-frequency VUV in this region is too weak as shown by the fact that the H₂O photoionization peak in the TOF spectrum has nearly disappeared.

The next $^{1}\Sigma^{+}$ band in Fig. 2 is the $(6p\sigma)^{1}\Sigma^{+}(v'=0)$ band at 109 177.2 cm $^{-1}$. The rotational assignments from Ref. 13 are shown as the drop lines in Fig. 2. The photofragment spectrum of this band is very weak but it shows rotational structure similar to the photoionization spectrum in Ref. 13, where they reported a predissociation lifetime that is less than 3×10^{-11} s. The line width of the R(0) line in this spectrum is 0.53 cm $^{-1}$ and by using Eq. (1) we obtain a lifetime for the

 $(6p\sigma)^1\Sigma^+(v'=0)$ state of 3.5×10^{-11} s. The two values are consistent within the experimental error of the measurements.

The two previously reported ${}^{1}\Sigma^{+}$ bands of $(4s\sigma){}^{1}\Sigma^{+}(v')$ = 4) $[(B^2\Sigma^+)3s\sigma, v' = 0]$ at 109452 cm^{-1} and $(4p\sigma)^1\Sigma^+(v')$ = 3) at 109 485 cm⁻¹ (Ref. 35) by us were also observed but will not be repeated here. Figure 3 shows the next strong $^{1}\Sigma^{+}$ band at 110 303 cm⁻¹ that is assigned as the $(7p\sigma)^1\Sigma^+(v')$ = 0) band. This Rydberg state was observed and labeled as 5 in the Table I of Ref. 45 and was assigned to the $np\sigma$ Rydberg series by Ogawa and Ogawa⁴⁶ based on their absorption spectrum. Its band origin and rotational constant were reported, respectively, as 110 299 cm⁻¹ and 1.82 cm⁻¹ by Komatsu et al. 15 in their ion-dip spectrum. This band was also seen in Okazaki's C(3P) photofragment yield spectrum with partially rotationally resolved structure. 16 We obtained rotationally resolved C⁺ photofragment spectrum for this band, the peak positions and assignments were showed by drop lines in Fig. 3 (left) and listed in Table I. This spectrum was used to determine a band origin of 110 299.1 cm⁻¹ and a rotational constant of 1.863 cm⁻¹ for this state. This is very close to Komatsu's results.15 The observed line width of the P(1) level which corresponds to J' = 0 level of the $(7p\sigma)^1 \Sigma^+(v' = 0)$ band is within our instrumental resolution of 0.45 cm⁻¹. Thus, the predissociation lifetime for this rotational level is longer than 1.2×10^{-11} s. From the spectrum shown in Fig. 3, we can see that the peak becomes broader as J' increases from 0 for the P(1) line to 4 for the R(3) line. Equation (1) is used to determine the lifetime of each of these J' levels from the line width, Γ (in cm⁻¹), for each of these lines, ⁴⁷

$$\Gamma = \delta \nu_{\text{obs}} - [(\delta \nu_{\text{instr}})^2 / \delta \nu_{\text{obs}}]_{-}, \tag{1}$$

where the $\delta\nu_{obs}$ is the observed line width, and the $\delta\nu_{instr}$ is the instrumental resolution, which is $0.45~cm^{-1}$ for our apparatus. We have obtained the natural predissociation line widths from R(0) to R(3) level and plotted them as a function of J(J+1) as shown in Fig. 5. The predissociation line width is linearly dependent on J(J+1), which implies that the $(7p\sigma)^1\Sigma^+(v'=0)$

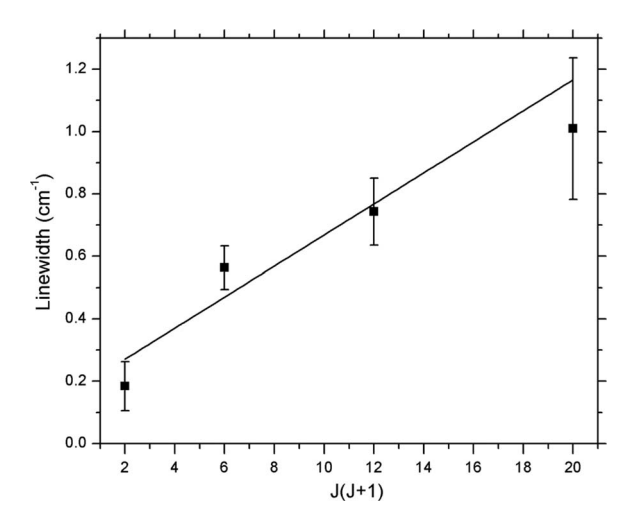


FIG. 5. Rotational state dependent predissociation line widths for the $(7p\sigma)^1\Sigma^+(v'=0)$ state as a function of J(J+1). The observed line width for the P(1) line, which corresponds to J=0 level, is the same as the instrumental resolution, thus we cannot obtain its natural predissociation line width from deconvolution of the observed line width.

TABLE I. Branching ratios of the Σ bands.

Band system	VUV (cm ⁻¹)	Rotation line	$C(^{1}D) + O(^{3}P)^{a} \%$	$C(^{3}P) + O(^{1}D) \%$	$C(^{3}P) + O(^{3}P) \%$
	108 154.9	R(0)	<1	<1	100
	108 158.5	R(1)	<1	<1	100
$^{1}\Sigma^{+}(v'=1)[(4d\sigma)^{1}\Sigma^{+}(v'=1)]$	108 162.1	R(2)	<1	<1	100
	108 147.4	P(1)	<1	<1	100
	108 143.5	P(2)	<1	<1	100
	108 370.0		<1	<1	100
$(5d\sigma)^{1} \Sigma^{+}(\mathbf{v}'=0)$ $(6p\sigma)^{1} \Sigma^{+}(\mathbf{v}'=0)$	108 373.5		<1	<1	100
	108 378.8		<1	<1	100
	109 177.2	R(0)	<5	<5	>90
	109 180.2	R(1)	<5	<5	>90
	109 170.1	P(1)	<5	<5	>90
	110 302.8	R(0)	1.7 ± 0.1^{b}	5.4 ± 0.3	93.0 ± 0.2
	110 306.4	R(1)	1.6 ± 0.1	4.8 ± 0.4	93.6 ± 0.4
	110 309.8	R(2)	1.7 ± 0.1	6.2 ± 1.1	92.2 ± 1.1
$(7p\sigma)^1 \Sigma^+(v'=0)$	110 312.9	R(3)	1.8 ± 0.1	7.1 ± 0.5	91.1 ± 0.5
	110 295.3	P(1)	1.2 ± 0.1	2.4 ± 0.3	96.4 ± 0.4
	110 291.3	P(2)	1.6 ± 0.1	5.5 ± 0.2	92.9 ± 0.2
	110 287.5	P(3)	1.7 ± 0.2	7.0 ± 0.8	91.3 ± 0.8

^aThe ratios to the channel of $C(^{1}D) + O(^{3}P)$ have been corrected for the photoionization cross sections of $C(^{3}P)$ and $C(^{1}D)$.

band predissociates through a heterogeneous perturbation by a repulsive state with Π symmetry. Which is observed at 110 290.5 cm⁻¹ on the red side of P(2) line (Fig. 3) is caused by the Kr single photon resonance line: $4s^24p^5(^2\text{Po}_{3/2})8d^2[1/2]^{\text{o}}_1 \leftarrow ^1\text{S}_0$. This phenomenon has been observed and explained in our NO experiment.

Besides the $^1\Sigma^+$ bands discussed above, an extra band near 109 040 cm $^{-1}$, that is labeled in Fig. 2 by a question mark shows rotational structure with $^1\Sigma^+$ characteristics. To our knowledge, this band, which is too weak to get good ion images, has never been observed before. It may be due to the $^1\Sigma^+$ analog band of the $^1\Pi$ band at 109 013 cm $^{-1}$ for which the time-slice ion image has been reported in our recent communication. Their electron configurations are only different by one electron (the Rydberg electron), and strongly coupled to each other. This may explain the nearly isotropic angular distribution for the band at 109 013 cm $^{-1}$ observed from our time-slice ion images. The strong shows the strong s

To measure the branching ratio, we have obtained the time-slice velocity-map ion images at the bands that have rotational lines strong enough when detecting the C⁺ ions. Examples of the raw images and the corresponding TKER spectra for the R(0) level of the band $^{1}\Sigma^{+}(v'=1)$ [$(4d\sigma)^{1}\Sigma^{+}$ (v' = 1)] at 108 154.9 cm⁻¹ and the R(0) level of the band $(7p\sigma)^{1}\Sigma^{+}(v'=0)$ at 110 302.8 cm⁻¹ are shown in Figs. 6(a) and 6(b) and 6(c) and 6(d), respectively. Three peaks near 0.6 eV, 1.3 eV, and 2.5 eV were observed in Fig. 6(d) and they are assigned to the three energetically available predissociation channels of CO, i.e., $C(^3P) + O(^1D)$, $C(^1D) + O(^3P)$, and $C(^{3}P) + O(^{3}P)$, respectively. The peak at 2.5 eV corresponding to the channel $C(^3P) + O(^3P)$ for the $(7p\sigma)^1\Sigma^+(v'=0)$ at $110\,302.8$ cm⁻¹ in Fig. 6(b) is shifted to about 2.2 eV for the band ${}^{1}\Sigma^{+}(v'=1)$ [$(4d\sigma)^{1}\Sigma^{+}$ (v'=1)] at 108 154.9 cm⁻¹ in Fig. 6(d). This observation confirms that the images are produced from the predissociation of CO following the absorption of a single sum-frequency VUV photon, i.e., $2\omega_1+\omega_2$ because the peak shift corresponds exactly to the energy difference of the two sum-frequency VUV photons. From the images and TKER spectra in Figs. 6(b) and 6(d), we can see that the channel producing $C(^3P) + O(^3P)$ dominates the predissociation process for both of the two bands, but in the TKER spectrum for the $(7p\sigma)^1\Sigma^+(v'=0)$ band, a small but measurable amount of CO can predissociate into $C(^3P) + O(^1D)$ and $C(^1D) + O(^3P)$ channels. In the TKER

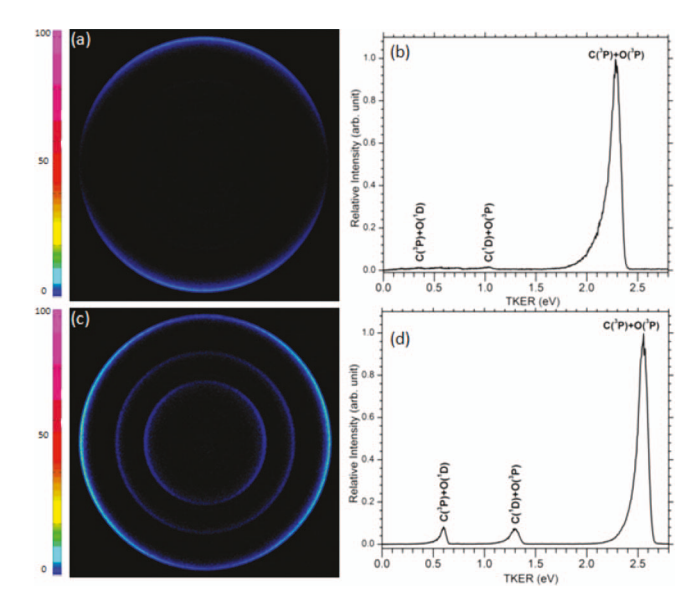


FIG. 6. Raw time-slice velocity-map ion images and their TKER spectra produced from the predissociation of CO following the absorption of a single sum-frequency VUV photon for the R(0) line of the band $^1\Sigma^+(v'=1)$ [(4d σ) $^1\Sigma^+(v'=1)$] ((a) and (b)) at 108 154.9 cm $^{-1}$ and the R(0) line of the band $(7p\sigma)^1\Sigma^+(v'=0)$ ((c) and (d)) at 110 302.8 cm $^{-1}$. The TKER spectra were normalized by treating the height of the C(3P) + O(3P) peak as 1. The assignments for each of the peaks are shown in (b) and (d).

^bThe standard errors are generated from three independent measurements.

We have measured the branching ratios for the three observed predissociation channels by integrating the areas under each of the three peaks for all the bands with strong C⁺ photofragment excitation spectra in this energy region and listed them in Table I. For the diffuse $(5d\sigma)^1\Sigma^+(v'=0)$ band, we have collected images both at the peak position and the positions with half intensity to make sure they are similar to each other. At each of the photon energy, we repeated the measurements at least three times to confirm their accuracy. As mentioned above, the intensity of the channel producing $C(^{1}D)$ has to be calibrated by considering the different photoionization cross sections between $C(^3P)$ and $C(^1D)$. The photoionization cross section of C(³P) has been previously calculated by both the R-matrix method^{51,52} and many-body perturbation theory.⁵³ It has also been measured experimentally by Cantu et al.54 The photoionization cross section of $C(^{3}P)$ was found to be about 16 Mb in the region we are studying here. The photoionization cross section of $C(^{1}D)$ has also been calculated before, 52,55 but no experimental measurement has been reported. According to the theoretical calculation, the photoionization cross section of $C(^{1}D)$ in this region depends dramatically on the excitation energy of the photon. The accuracy of the theoretical calculations is low, thus it is one of the biggest sources of uncertainty in our experimental measurements of the branching ratios. Based on the calculation results, 52,55 we used photoionization cross sections of 30 Mb, 50 Mb, and 60 Mb, respectively, for ${}^{1}\Sigma^{+}(v')$ = 1) $[(4d\sigma)^1 \Sigma^+ (v' = 1)]$ and $(5d\sigma)^1 \Sigma^+ (v' = 0)$, $(6p\sigma)^{1}\Sigma^{+}(v'=0), (7p\sigma)^{1}\Sigma^{+}(v'=0)$ bands. To get a more accurate calibration, detailed and accurate measurements of the photoionization cross section of $C(^1D)$ are needed, or an independent method needs to be employed.

From Table I, we can see that the first three $^1\Sigma^+$ bands do not produce signals strong enough for accurate branching ratio measurements of the two spin-forbidden channels, so only upper limits are listed in the table. This implies that the predissociation channels producing $C(^1D) + O(^3P)$ and $C(^3P) + O(^1D)$ are not very likely for these three $^1\Sigma^+$ bands. For the $(7p\sigma)^1\Sigma^+(v'=0)$ band, observable percentages into the two spin-forbidden channels can be obtained and are listed in Table I. The true error in the branching ratios measured for the $(7p\sigma)^1\Sigma^+(v'=0)$ from the same J' level is larger than the statistical error in Table I. This could be due to either the different signal sizes for different branches or other interferences at the two different wavelengths.

B. ¹Π bands

Recently, we have reported on the C⁺ ion photofragment spectra and the branching ratios in the predissociation for two ${}^{1}\Pi$ bands at 108014 cm ${}^{-1}$ and 109019 cm ${}^{-1}$. 35 These two bands were listed as $W(3s\sigma)^1\Pi(v=3)$ and $^1\Pi(v=2)$ $[(A^2\Pi)3s\sigma \ v'=3]$, respectively, in Table I of Ref. 5. The next ${}^{1}\Pi$ band, $(6p\pi){}^{1}\Pi(v=0)$, is diffuse and should be observed at 109 203 cm⁻¹ (Ref. 5) according to Eidelsberg and Rostas.³ We see a very broad and weak structure (not shown here) corresponding to this band in our C⁺ ion photofragment spectrum but it is not strong enough to collect ion images. The next ${}^{1}\Pi$ band $(5p\pi){}^{1}\Pi(v=1)$ overlaps with two strong $^{1}\Sigma^{+}$ bands 18 and cannot be uniquely identified in our C^{+} photofragment spectrum.³⁵ Eidelsberg et al.¹⁸ have assigned the band at 109 564 cm⁻¹ in the C⁺ ion photofragment spectrum shown in Fig. 4 to the $(4p\pi)^1\Pi(v'=3)$ [(A² Π) $3p\sigma$ v' = 0] Rydberg state. The rotational assignments are designated by the drop lines and the line positions are consistent with the studies of both Eikema et al. 13 and those of Eidelsberg et al. 18 The next ${}^{1}\Pi$ band in the C^{+} ion photofragment spectrum is due to the $(7p\pi)^{1}\Pi$ (v' = 0), which is at 110 345 cm⁻¹ in Fig. 3. This band was first identified in the absorption spectrum by Ogawa et al. 46 at 110 331 cm⁻¹, and then observed in the ion-dip spectrum by Komatsu et al. 15 at $110\,350\,\mathrm{cm}^{-1}$ and in the C(³P) ion yield spectrum by Okazaki et al. 16 at ~ 110349 cm $^{-1}$. According to the C⁺ ion photofragment spectrum in Fig. 3, this band is strongly broadened due to a fast predissociation process. The relative intensity is much smaller than its analog state $(7p\sigma)^1 \Sigma^+(v'=0)$. This is contrary to the C(³P) ion yield spectrum obtained by Okazaki et al. 16 where the sigma and pi states have comparable intensities. This may be due to the fact that they used a multi-photon excitation scheme that can have different excitation probability than a single photon excitation process.

Besides the previously identified $^1\Pi$ bands discussed above, there are two extra bands at 108 988 cm $^{-1}$ and 110 480 cm $^{-1}$ shown in Figs. 2 and 3 that also seem to have $^1\Pi$ character. The anisotropy parameters for the production of the $C(^3P) + O(^3P)$ channel from these two band were measured as -0.12 and -0.48, respectively. To our knowledge, the band at 108 988 cm $^{-1}$ has not been observed before, and the band

Band system	VUV (cm ⁻¹)	Rotation line	$C(^{1}D) + O(^{3}P)^{a} \%$	$C(^{3}P) + O(^{1}D) \%$	$C(^{3}P) + O(^{3}P) \%$
$1\Pi (v'=?)$	108 988.0		$20 \pm 4^{\text{b}}$	21 ± 8	59 ± 5
	109 564.5	Q(1)	22 ± 2	30 ± 4	48 ± 3
$(4p\pi)^1\Pi(v'=3)$	109 568.6	R(0)	22 ± 1	30 ± 3	48 ± 2
$[(A^2\Pi)3p\sigma \ v'=0]$	109 572.3	R(1)	21 ± 3	31 ± 6	49 ± 4
	109 576.3	R(2)	19 ± 2	26 ± 3	55 ± 2
$(7p\pi)^1\Pi(\mathbf{v}'=0)$	110 345.1	Q(1)	3.2 ± 0.1	17.1 ± 1.0	79.7 ± 1.0
	110 349.4	R(0)	3.0 ± 0.1	18.0 ± 1.0	79.0 ± 1.0
$^{1}\Pi (v'=?)$	110 479.1		1.4 ± 0.2	3.1 ± 0.1	95.5 ± 0.3
$[[(A^2\Pi)3s\sigma \ v'=4]$	110 485.5		1.4 ± 0.1	2.7 ± 0.6	96.0 ± 0.7

^aThe ratios to the channel of $C(^1D) + O(^3P)$ have been corrected for the photoionization cross sections of $C(^3P)$ and $C(^1D)$.

at $110\,480\,\mathrm{cm^{-1}}$ was observed in the absorption spectrum by Letzelter *et al.* at 90.509 nm, i.e., $110\,486\,\mathrm{cm^{-1}}.^{45}$ It was previously assigned as $(\mathrm{A^2\Pi})\,3s\sigma$ (v' = 4) by Casey. An accurate assignment needs more detailed information of CO over a larger spectral range.

To measure the branching ratios of the $^1\Pi$ bands, we have obtained the time-slice velocity-map ion images by detecting C⁺ ions. Examples of the raw images and the corresponding TKER spectra for the R(0) line of the band $(4p\pi)^1\Pi(v'=3)$ [(A² Π) $3p\sigma$ v'=0] at 109 568.6 cm⁻¹ and the Q branch of the band $(7p\pi)^1\Pi(v'=0)$ at 110 345.1 cm⁻¹ are shown in Fig. 7. Again these two $^1\Pi$ bands have very different branching ratios. The percentages for the spin-forbidden channels for the $(4p\pi)^1\Pi(v'=3)$ [(A² Π) $3p\sigma$ v'=0] band are much larger than those for the band of $(7p\pi)^1\Pi(v'=0)$. The angular distribution of the $(4p\pi)^1\Pi(v'=3)$ [(A² Π) $3p\sigma$ v'=0] band is strongly perpendicular with a recoil anisotropy parameter of

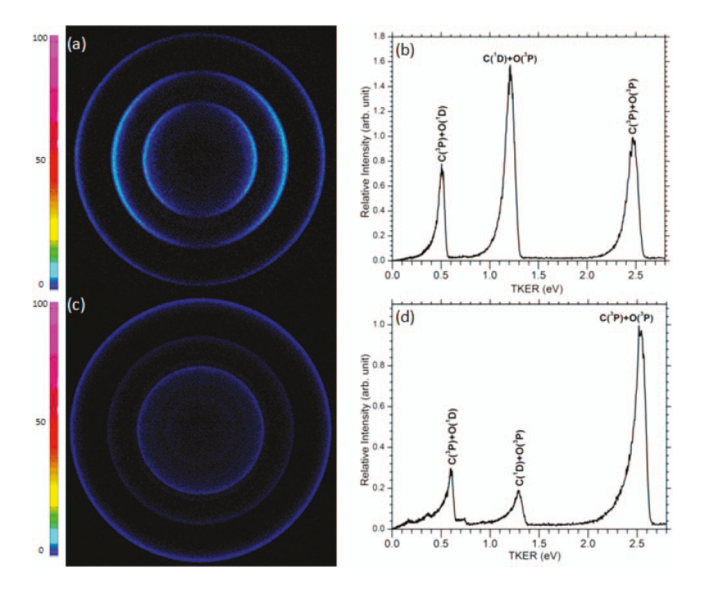


FIG. 7. Raw time-slice velocity-map ion images and their TKER spectra produced from the predissociation of CO following the absorption of a single sum-frequency VUV photon for the R(0) line of the band $(4\rho\pi)^1\Pi(v'=3)$ [(A² Π) $3\rho\sigma$ v'=0] ((a) and (b)) at 109 568.6 cm⁻¹ and the Q branch of the band $(7\rho\pi)^1\Pi(v'=0)$ ((c) and (d)) at 110 345.1 cm⁻¹. The TKER spectra were normalized by treating the height of the C(³P) + O(³P) peak as 1. The assignments for each of the peaks are shown in (b) and (d).

-0.8, which is consistent with a Σ-Π transition. The recoil anisotropy parameter for the R(0) line of the $(7p\pi)^1\Pi(v'=0)$ band at 110 349.4 cm⁻¹ is -0.5. This is a large deviation from -1 and it could indicate that predissociation is slower or that there is a larger mixture of the $(7p\pi)^1\Pi(v'=0)$ with its $^1\Sigma^+$ analog band $(7p\sigma)^1\Sigma^+(v'=0)$ as mentioned above.

The branching ratios for all the $^1\Pi$ bands are measured from their time-slice velocity-map ion images and they are listed in Table II. A photoionization cross section for the C(3P) atoms of 16 Mb is used for these measurements. For the C(1D) atoms a photoionization cross section of 50 Mb is used for the bands at 108 988 cm $^{-1}$ and 109 564 cm $^{-1}$, and 60 Mb for the bands at 110 345 cm $^{-1}$ and 110 480 cm $^{-1}$. Again, from Table II, we see that the branching ratios in the predissociation of CO strongly depend upon which state is being excited.

IV. DISCUSSION AND CONCLUSION

The above measurements and the results reported in our recent communication³⁵ for the branching ratios for the predissociation of CO molecules can be used to determine how the states of the atomic products vary with the single photon excitation energy. The percentages of the three dissociation channels versus the single photon excitation energy for all the $^{1}\Pi$ bands and $^{1}\Sigma^{+}$ bands are plotted in Figs. 8(a) and 8(b), respectively. In the present study, we are above the dissociation energies for the singlet and triplet channels at all of the wavelengths used in the present study. From the figure, we can conclude that the branching ratio into different channels for the dissociation of CO is strongly dependent on exactly what VUV excitation energy is used. This is highly suggestive that the wavelength dependence can be used to determine the energy where there is a high probability for intersystem crossing to triplet states that lead to dissociation. The present points are too sparse to clearly define these crossing points so more work will be needed.

In Fig. 8, we see that there are bands that predissociate into the two spin-forbidden channels and in some cases they are of the same order of magnitude as the allowed channel. This is not the only region where the ground and excited fragments are produced with comparable yields. Okazaki *et al.* have shown that the $C(^{1}D)$ channel is produced with

^bThe standard errors are generated from three independent measurements.

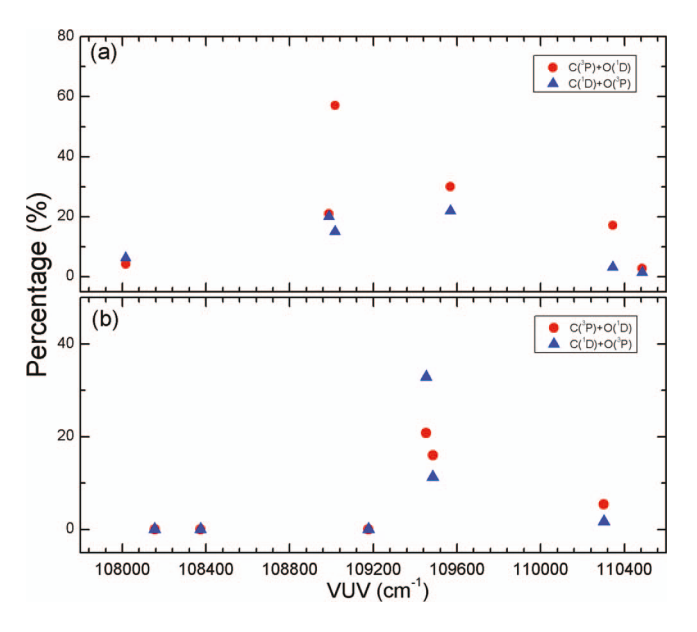


FIG. 8. The plot of the branching ratio for the predissociation of CO versus the single photon excitation energy: (a) Π bands, (b) Σ bands. The percentages into the channels producing $C(^1D) + O(^3P)$ and $C(^3P) + O(^1D)$ are plotted with red circle and blue triangle, respectively. The error bars are smaller than the symbols for most of the data points.

comparable intensity with that of C(³P) channel for the $L(4p\pi)^1\Pi$ (v = 0) band at 103 270 cm⁻¹. ^{16,33} This is below the threshold energy for the production of the O(¹D) that we observe in the present study. Excited singlet states cannot correlate to the spin-forbidden triplet dissociation channels but they must undergo intersystem crossing to a triplet state first. Based upon the present branching ratio measurements, spinorbit interactions are greatly enhanced for certain states in this region. The branching ratios dependence on the excitation energy between $N(^2D^0) + N(^4S)$ and $N(^2P^0) + N(^4S)$ for N_2 can be qualitatively explained by the structures of the three lowest adiabatic ${}^{3}\Pi$ states and their interactions with the singlet states.^{56,57} However, similar information for the ³Π Rydberg and valence states of CO is not presently available. Yet this information is crucial for understanding the predissociation dynamics of CO into the spin-forbidden triplet channels.

The dynamics for the $C(^3P) + O(^3P)$ singlet dissociation channel has been explained invoking an interaction with the repulsive $D'^1\Sigma^+$ state in several studies. 9, 13, 19-22 Eidelsberg et al. extended this explanation to higher regions for the $^{1}\Sigma^{+}$ states by using a complex mixture of $B^1\Sigma^+$ (v' = 6, 7, 9) and the repulsive $D'^{1}\Sigma^{+}$ state. This complex mixture of states will also play an important role for the production of the $C(^{3}P) + O(^{3}P)$ channel in the present study, especially for the three lowest ${}^{1}\Sigma^{+}$ bands observed here where only the ground dissociation channel is present. The ${}^{1}\Pi$ valence state that correlates to the ground dissociation channel was first assigned by O'Neil et al. 58, and later identified as the $2^{1}\Pi$ state by Cooper et al. Lefebvre-Brion and co-workers have done very detailed theoretical calculations on the adiabatic potential curves of the valence ${}^{1}\Pi$ states. 7,10,59 The ${}^{3}\Pi$ valence states correlating to the ground dissociation channel have also been calculated by O'Neil et al.⁵⁸ and recently in much more detail by Lefebvre-Brion and co-workers.^{7,10} The role of the valence $k^3\Pi$ state in the predissociation mechanism has been mentioned above, and it has been recently confirmed by Lefebvre-Brion and co-workers' ab initio calculations. 10 Besides the above investigations, the dynamics of the Π valence states for the production of the $C(^{3}P) + O(^{3}P)$ channel is not as clear as the dynamics from the $D'^1\Sigma^+$ state. The role of these Π states in the production for the ground dissociation channel has been confirmed by the line width measurements for the $(7p\sigma)^1 \Sigma^+(v'=0)$ state in Fig. 5. As discussed above, a linear rotational dependence of the line width on the J(J+1) implies that it is being predissociated by a nearly repulsive state with Π symmetry, and this state has been shown to produce mainly the ground atomic fragments in Table I. Further study is needed to understand the role of the Π valence states in the dynamics for producing the $C(^{3}P) + O(^{3}P)$

A detailed global picture for the production of the two lowest spin-forbidden triplet channels has not yet been established. Because only triplet states can correlate to those channels, the directly photo-excited singlet states have to couple to certain triplet states through intersystem crossing to dissociate. The spin-orbit interaction between ${}^{1}\Pi$ and ${}^{3}\Pi$ states are the key point in the predissociation dynamics of the ${}^{1}\Pi$ states of N_2 ,⁶⁰ and the $^1\Sigma^+$ states may have to couple to $^1\Pi$ states first to predissociate. 61 The spin-orbit interaction between the lowest ${}^{1}\Pi$ and ${}^{3}\Pi$ states of CO has been studied theoretically by Hall et al. in 1973, and they found that the perturbation is strongly dependent on the inter-nuclear distance and the vibrational states.⁶² In recent calculations of the potential energy curves of CO by Lefebvre-Brion et al., 10 the adiabatic potential curves with the $^{3}\Pi$ character have been obtained and shown in Fig. 4 of Ref. 10. They are similar to the $^{3}\Pi$ states of N2. The adiabatic curves are formed by several diabatic Rydberg and valence ${}^{3}\Pi$ states through many avoided crossings. The relative strengths of those avoided crossings to different repulsive ${}^{3}\Pi$ curves are probably responsible for the strong state-dependent branching ratios for the predissociation of CO measured in the present study. The single photon excited ${}^{1}\Pi$ states should couple to certain ${}^{3}\Pi$ states of either Rydberg or valence types through the spin-orbit interaction, these ${}^{3}\Pi$ states will predissociate through avoided crossings with repulsive ${}^{3}\Pi$ states, which correlate to the two triplet channels. The spin-orbit interaction is enhanced for certain states in the region from 108 900 cm⁻¹ to 109 600 cm⁻¹, which increases the yield to the two spin-forbidden triplet channels. This is probably because certain ${}^{3}\Pi$ states are crossing with those singlet states in this wavelength region. The $^{1}\Sigma^{+}$ states may have to couple to $^{1}\Pi$ states as a first step through heterogeneous interactions to predissociate into the spin-forbidden triplet channels, and this may explain the fact that most of the ${}^{1}\Sigma^{+}$ states in the present study only predissociate into the ground channel. The $(4s\sigma)^1\Sigma^+(v'=4)$ $[(B^2\Sigma^+)3s\sigma, v'=0]$ and $(4p\sigma)^1\Sigma^+(v'=3)$ bands produce comparable amounts of excited atomic fragments with the ground state atoms.³⁵ Eidelsberg et al. showed that the $(4p\sigma)^1\Sigma^+(v'=3)$ band interacts with the $(4p\pi)^1\Pi^+(v'=1)$ 3) $[(A^2\Pi) 3p\sigma v' = 0]$ band and another dark ${}^1\Pi$ band in this region, and the two ${}^{1}\Sigma^{+}$ bands strongly couple to each

other. ¹⁸ Based on the observations that predissociation of ${}^{1}\Pi$ bands in this region produce comparable amount of excited atoms, then the interaction of $(4s\sigma)^{1}\Sigma^{+}(v'=4)$ [(B² Σ^{+})3s σ , v'=0] and $(4p\sigma)^{1}\Sigma^{+}(v'=3)$ states with nearby ${}^{1}\Pi$ states would explain the very high yields into the spin-forbidden channels.

If we accept the assignments made by Casey in his Ph.D. dissertation,⁴⁴ an interesting phenomenon can be noticed. According to Casey, the levels at 108 016 cm⁻¹, 109 017 cm⁻¹, 109 568 cm⁻¹, and 110 480 cm⁻¹ can be assigned as Rydberg states converging to the ionic core $CO^+(A^2\Pi)$. The level at 109 452 cm⁻¹ was assigned as a Rydberg state converging to the ionic core $CO^+(B^2\Sigma^+)$. Several levels surrounding this level have high yields of spin-forbidden channels. We speculate that the presence of a Rydberg state with a (B ${}^{2}\Sigma^{+}$) ionic core enhances the spin-orbit coupling to these spin-forbidden channels. If this is the case, then we would expect that the Rydberg levels associated with the (B $^{2}\Sigma^{+}$) will have a higher yield for the spin-forbidden channels compared to those converging to the $(A^2\Pi)$ ionic core and the ground ionic core. The $(4s\sigma)^1\Sigma^+(v'=4)$ [$(B^2\Sigma^+)3s\sigma$, v' = 0] band at 109 452.5 cm⁻¹ and the $(4p\sigma)^1\Sigma^+(v' = 3)$ band at 109 484.7 cm⁻¹ from our earlier study³⁵ certainly follow this expectation since their yields of the spin-forbidden channels are much higher than the yields from most of the states with an $(A^2\Pi)$ ionic core and ground ionic core that are not near the Rydberg state with the (B $^{2}\Sigma^{+}$) ionic core. The three states out of 12 that we have studied so far that deviate from this trend are the unidentified state ${}^{1}\Pi$ at $108\,988\,\mathrm{cm}^{-1}$, another ${}^{1}\Pi^{+}(v'=2)$ state³⁵ at $109\,016.9\,\mathrm{cm}^{-1}$ and the $(4p\pi)^{1}\Pi(v'=3)$ [(A² Π) $3p\sigma$ v'=0] band at 109 564.5 cm⁻¹. This is analogous to the results from Helene Lefebvre-Brion that showed that the spin-orbit mixing between ${}^{1}\Pi$ and ${}^{3}\Pi$ Rydberg states with $A^{2}\Pi$ ionic core is more important than the mixing between those states with $X^{2}\Sigma^{+}$ ionic core.⁶³ In the present case, the addition of the nearby Rydberg state with a $(B^2\Sigma^+)$ ionic core increases the coupling to the triplet states. To confirm this, a more systematic study of the branching ratios in a larger energy range will be needed.

In summary, we have combined the time-slice velocitymap ion imaging and the resonant four-wave mixing techniques to measure the branching ratio of the CO predissociation into the three lowest channels in the region from $108\,000\,\mathrm{cm^{-1}}$ (92.59 nm) to $110\,500\,\mathrm{cm^{-1}}$ (90.50 nm) by using only one windowless VUV beam. Our reported branching ratios are dependent on the previously measured and/or calculated photoionization cross sections of $C(^3P)$ and $C(^1D)$. To make a more accurate measurement and to determine the crossing points, two separate VUV beams are needed, so that we can probe specifically $C(^{3}P)$ or $O(^{3}P)$ by fixing one VUV beam to match one of the resonance lines of those atoms and scan the other VUV beam for dissociation. This will increase the sensitivity for detection and is part of our future plans. In the present study, a tentative explanation for the observation has been given. The ${}^{3}\Pi$ states with Rydberg or valence types and their spin-orbit interactions with the ${}^{1}\Pi$ states play important roles in the dynamics for producing the spin-forbidden triplet channels. More detailed and quantitative theoretical calculations are definitely needed to explain the observation in the present study.

ACKNOWLEDGMENTS

H. Gao, Yu Song, and W. M. Jackson were supported by National Science Foundation (NSF) under Grant No. CHE-0957872. H. Gao, L. Yang, and C. Y. Ng were supported by NASA under Grant No. 07-PATM07-0012, (U.S.) Department of Energy (DOE) on Contract No. DEFG02-02ER15306 and NSF on Grant No. CHE 0910488. C. Y. Ng, Xiaoyu Shi, and Qingzhu Yin were supported by NASA Origins of Solar Systems Program Grant No. NNX09AC93G.

- ¹M. Yan, A. Dalgarno, W. Klemperer, and A. E. S. Miller, Mon. Not. R. Astron. Soc. **313**(2), L17 (2000).
- ²F. Bertoldi, P. Cox, R. Neri, C. L. Carilli, F. Walter, A. Omont, A. Beelen, C. Henkel, X. Fan, Michael A. Strauss, and K. M. Menten, Astron. Astrophys. 409, L47 (2003).
- ³M. Eidelsberg and F. Rostas, Astron. Astrophys. **235**(1–2), 472 (1990).
- ⁴M. Eidelsberg, Y. Sheffer, S. R. Federman, J. L. Lemaire, J. H. Fillion, F. Rostas, and J. Ruiz, Astrophys. J. **647**(2), 1543 (2006).
- ⁵R. Visser, E. F. van Dishoeck, and J. H. Black, Astron. Astrophys. **503**(2), 323 (2009)
- ⁶K. P. Huber, Philos. Trans. R. Soc. London, Ser. A **355**(1729), 1527 (1997).
- ⁷H. Lefebvre-Brion and B. R. Lewis, Mol. Phys. **105**(11–12), 1625 (2007).
- ⁸G. L. Wolk and J. W. Rich, J. Chem. Phys. **79**, 12 (1983).
- ⁹D. L. Copper and K. Kirby, J. Chem. Phys. **87**, 424 (1987).
- ¹⁰G. J. Vázquez, J. M. Amero, H. P. Liebermann, and H. Lefebvre-Brion, J. Phys. Chem. A **113**(47), 13395 (2009).
- ¹¹M. Drabbels, J. Heinze, J. J. Termeulen, and W. L. Meerts, J. Chem. Phys. **99**(8), 5701 (1993).
- ¹²M. Komatsu, T. Ebata, and N. Mikami, J. Chem. Phys. **99**, 9350 (1993).
- ¹³K. S. E. Eikema, W. Hogervorst, and W. Ubachs, Chem. Phys. **181**(1–2), 217 (1994).
- ¹⁴F. Rostas, F. Launay, M. Eidelsberg, M. Benharrous, C. Blaess, and K. P. Huber, Can. J. Phys. **72**(11–12), 913 (1994).
- ¹⁵M. Komatsu, T. Ebata, T. Maeyama, and N. Mikami, J. Chem. Phys. 103, 2420 (1995).
- ¹⁶A. Okazaki, T. Ebata, and N. Mikami, J. Chem. Phys. 114(18), 7886 (2001).
- ¹⁷P. Cacciani, F. Brandi, J. P. Sprengers, A. Johansson, A. L'Huillier, C. G. Wahlström, and W. Ubachs, Chem. Phys. 282(1), 63 (2002).
- ¹⁸M. Eidelsberg, F. Launay, K. Ito, T. Matsui, P. C. Hinnen, E. Reinhold, W. Ubachs, and K. P. Huber, J. Chem. Phys. **121**(1), 292 (2004).
- ¹⁹W. U. L. Tchang-Brillet, P. S. Julienne, J. M. Robbe, C. Letzelter, and F. Rostas, J. Chem. Phys. **96**(9), 6735 (1992).
- ²⁰M. Monnerville and J. M. Robbe, J. Chem. Phys. **101**(9), 7580 (1994).
- ²¹Y. Li, O. Bludsky, G. Hirsch, and R. J. Buenker, J. Chem. Phys. **107**(8), 3014 (1997).
- ²²L. Andric, F. Bouakline, T. P. Grozdanov, and R. McCarroll, Astron. Astrophys. 421, 381 (2004).
- ²³K. Kirby and D. L. Copper, J. Chem. Phys. **90**, 4895 (1989).
- ²⁴David L. Copper and K. Kirby, Chem. Phys. Lett. **152**, 393 (1988).
- ²⁵M. Eidelsberg, J. L. Lemaire, S. R. Federman, G. Stark, A. N. Heays, Y. Sheffer, L. Gavilan, J.-H. Fillion, F. Rostas, J. R. Lyons, P. L. Smith, N. de Oliveira, D. Joyeux, M. Roudjane, and L. Nahon, "High-resolution study of oscillator strengths and predissociation rates for 12C16O: W-X bands and Rydberg complexes between 92.9 and 93.4 nm," Astron. Astrophys. (submitted).
- ²⁶J. Baker, J. L. Lemaire, S. Couris, A. Vient, D. Malmasson, and F. Rostas, Chem. Phys. **178**(1–3), 569 (1993).
- ²⁷G. Berden, R. T. Jongma, D. van der Zande, and G. Meijer, J. Chem. Phys. 107(20), 8303 (1997).
- ²⁸J. Baker, J. Mol. Spectrosc. **167**(2), 323 (1994).
- ²⁹J. Baker and F. Launay, J. Chem. Phys. **123**(23), 234302 (2005).
- ³⁰P. Cacciani, W. Hogervorst, and W. Ubachs, J. Chem. Phys. **102**(21), 8308 (1995).
- ³¹W. Ubachs, I. Velchev, and P. Cacciani, J. Chem. Phys. **113**(2), 547 (2000).
- ³²W. T. Hill III, B. P. Turner, H. Lefebvre-Brion, S. Yang, and J. Zhu, J. Chem. Phys. **92**(7), 4272 (1990).

- ³³ A. Okazaki, T. Ebata, T. Sutani, and N. Mikami, J. Chem. Phys. **108**(5), 1765 (1998).
- ³⁴B. L. G. Bakker and D. H. Parker, Chem. Phys. Lett. **330**(3–4), 293 (2000).
- ³⁵H. Gao, Y. Song, L. Yang, X. Shi, Q. Yin, C. Y. Ng, and W. M. Jackson, J. Chem. Phys. 135(22), 221101 (2011) (Communication).
- ³⁶X. Shi *et al.*, "Branching ratios of atomic states formed in vacuum ultraviolet induced predissociation of CO and N2: implications for oxygen and nitrogen isotope evolution in the early solar system," Astro. Phys. J. (submitted).
- ³⁷Y. Pan, H. Gao, L. Yang, J. Zhou, C. Y. Ng, and W. M. Jackson, J. Chem. Phys. **135**, 071101 (2011) (Communication).
- ³⁸ H. Gao, L. Yang, Y. Pan, J. Zhou, C. Y. Ng, and W. M. Jackson, J. Chem. Phys. **135**, 134319 (2011).
- ³⁹ H. Gao, Y. Pan, L. Yang, J. Zhou, C. Y. Ng, and W. M. Jackson, J. Chem. Phys. **136**(13), 134302 (2012).
- ⁴⁰J. Zhou, K.-C. Lau, E. Hassanein, H. Xu, S.-X. Tian, B. Jones, and C. Y. Ng, J. Chem. Phys. **124**, 034309 (2006).
- ⁴¹J. Zhou, B. Jones, X. Yang, W. M. Jackson, and C. Y. Ng, J. Chem. Phys. 128, 014305 (2008).
- ⁴²B. Jones, J. Zhou, L. Yang, and C. Y. Ng, Rev. Sci. Instrum. **79**, 123106 (2008).
- ⁴³G. N. Haddad and J. A. R. Samson, J. Chem. Phys. **84**(12), 6623 (1986)
- ⁴⁴M. Casey, Ph.D. dissertation, University College Dublin, 1979.
- ⁴⁵C. Letzelter, M. Eidelsberg, F. Rostas, J. Breton, and B. Thieblemont, Chem. Phys. 114(2), 273 (1987).

- ⁴⁶M. Ogawa and S. Ogawa, J. Mol. Spectrosc. **41**, 393 (1972).
- ⁴⁷S. N. Dobryakov and Y. S. Lebedev, Sov. Phys. Dokl. **13**, 873 (1969).
- ⁴⁸ H. Lefebvre-Brion and R. W. Field, *The Spectra and Dynamics of Diatomic Molecules* (Elsevier, 2004).
- ⁴⁹R. N. Zare and D. R. Herschbach, *Proc. IEEE* **51**, 173 (1963).
- ⁵⁰R. N. Zare, Angular Momentum: Understanding Spatial Aspects in Chemistry and Physics (Wiley, New York, 1988).
- ⁵¹K. T. Taylor and P. G. Burke, J. Phys. B: At., Mol. Opt. Phys. 9, L353 (1976).
- ⁵²P. G. Burke and K. T. Taylor, J. Phys. B **12**(18), 2971 (1979).
- ⁵³S. L. Carter and H. P. Kelly, *Phys. Rev. A* **13**, 1388 (1976).
- ⁵⁴ A. W. Cantu, M. Mazzoni, M. Pettini, and G. P. Tozzi, Phys. Rev. A 23, 1223 (1981).
- ⁵⁵H. Hofmann, H. P. Saha, and E. Trefftz, Astron. Astrophys. **126**(2), 415 (1983).
- ⁵⁶H. Helm and P. C. Cosby, J. Chem. Phys. **90**(8), 4208 (1989).
- ⁵⁷C. W. Walter, P. C. Cosby, and H. Helm, J. Chem. Phys. **99**(5), 3553 (1993).
- ⁵⁸S. V. O'Neil and H. F. Schaefer III, J. Chem. Phys. **53**(10), 3994 (1970).
- ⁵⁹H. Lefebvre-Brion, H. P. Liebermann, and G. J. Vazquez, J. Chem. Phys. 132(2), 024311 (2010).
- ⁶⁰B. R. Lewis, S. T. Gibson, W. Zhang, H. Lefebvre-Brion, and J. M. Robbe, J. Chem. Phys. **122**(14), 144302 (2005).
- ⁶¹M. O. Vieitez, T. I. Ivanov, W. Ubachs, B. R. Lewis, and C. A. de Lange, J. Mol. Liq. **141**(3), 110 (2008).
- ⁶²J. A. Hall, J. Schamps, J. M. Robbe, and H. Lefebvre-Brion, J. Chem. Phys. 59(6), 3271 (1973).
- ⁶³H. Lefebvre-Brion, private communication (May 21, 2012).